Polyurethane−Polyacrylate Interpenetrating Networks. 2. Morphology Studies by Direct Nonradiative Energy Transfer Experiments

Jie Yang and Mitchell A. Winnik*

Department of Chemistry and Erindale College, University of Toronto, Toronto, Canada M5S 1A1

David Ylitalo and Robert J. DeVoe

3M Corporate Research Laboratories, St. Paul, Minnesota 55144-1000

Received January 30, 1996; Revised Manuscript Received May 6, 1996[⊗]

ABSTRACT: Two sequential urethane−acrylate interpenetrating network (IPN) systems were prepared in which the polyurethane (PU) phase is labeled with donor and acceptor dyes. Direct nonradiative energy transfer (DET) measurements on these systems indicate less efficient energy transfer in the IPN than in the corresponding pure PU matrix. This result is interpreted in terms of dilution of the dyes by mixing at the molecular level between the polyacrylate (PA) and PU components. Quantitative analysis of the changes in DET efficiency allows the extent of phase mixing to be calculated. The two SeqIPN's, $PU_{g15}^{75\%}PA(EHA)^{100\%}PU^{100\%}$ and $PU_{g180}^{100\%}PA(IBA)^{100\%}$, were labeled by incorporating phenanthrene and anthracene diols into the reaction mixture. Fluorescence decays of phenanthrene in these samples were measured by the single-photon-timing technique and analyzed in terms of both the Förster model for DET and the Perrin model for static quenching. Both analyses gave similar extents of phase mixing, and these values are in good accord with the results of electron microscopy and dynamic mechanical experiments. Similar experiments were carried out during the polymerization reaction. These allowed features of the morphology evolution to be understood.

Introduction

In the preceding paper,[1] we described the preparation and global morphology of three different urethane−acrylate interpenetrating network (IPN) systems prepared from the same mixture of monomers. These IPN's, all containing 67 wt % urethane and 33 wt % acrylate, differ only in the order in which the various monomers were polymerized. When the acrylate was polymerized first, by photoinitiation using 2,2-dimethoxy-2-phenylacetophenone as the photoinitiator, large (100−300 nm) globular polyacrylate domains were observed as the dispersed phase in a continuous polyurethane matrix (SeqIPN $PA(EHA)^{100\%}PU^{100\%}$; cf. Figure 3B in the preceding paper[1]). When the urethane phase was first polymerized prior to the gel point (ca. 50% consumption of NCO groups by infrared spectroscopy), followed by photopolymerization of the acrylate and then thermal polymerization to completion of the urethane, somewhat smaller acrylate domains were observed by transmission electron microscopy (TEM) (SimIPN $PU^{50\%}PA(EHA)^{100\%}PU^{100\%}$; cf. Figure 3C in the preceding paper[1]). Here the domains were less regular in shape and the phase boundaries appeared to be more diffuse. Finally, if the urethane component was first polymerized to ca. 75% completion (i.e. with 25% of the NCO peak intensity remaining in the IR spectrum), then irradiated to photopolymerize the acrylate, and finally allowed to cure at room temperature until complete disappearance of the NCO groups from the IR spectrum, a different morphology was obtained.

This cure protocol yielded a transparent matrix with very small (<20 nm) polyacrylate domains seen by TEM (cf. Figure 3A in the preceding paper[1]). We refer to the polymer prepared in this way as SeqIPN $PU_{g15}^{75\%}PA(EHA)^{100\%}PU^{100\%}$. In Part 1 we examined the morphology of this sample in more detail by labeling it with fluorescent dyes and carrying out energy transfer experiments. In Part 2, we describe DET experiments on labeled samples of SeqIPN $PU_{g180}^{100\%}PA(IBA)^{100\%}$, which is a close analog of SeqIPN $PU_{g15}^{75\%}PA(EHA)^{100\%}PU^{100\%}$. We study the degree of phase mixing at both the intermediate stage and the final stage of IPN formation. Here the degree of mixing can be compared with that obtained from shifts in the glass transition temperature (T_g) of the components using the Fox equation as described in the preceding paper.[1] Appendix A of that paper describes the notation for the IPN systems, and Appendix I in this paper explains more about fluorescent labels in these IPN samples.

We would like to emphasize at the ouset that the objective of such experiments in a system of this complexity is to obtain new insights into the structure. Fluorescence and fluorescence decay experiments, like scattering experiments, need a model in order to be interpreted rigorously. In the sense that scattering experiments can provide information about surface area in a two-component blend without reference to a detailed model, direct nonradiative energy transfer (DET) measurements can provide information about mixing.

In the experiments described here, the urethane phase is labeled with both the energy donor (phenanthrene, Phe) and the energy acceptor (anthracene, An). Previous experiments from our laboratory have shown that in the absence of a second component, the dyes attached to the polyurethane (PU) undergo energy transfer in a manner completely in accord with both Förster kinetics and the Perrin model for static quenching.[2] These results establish the baseline for comparing the influence of the second component, the acrylate, on the DET kinetics. Significant changes do occur, and we

* To whom correspondence should be addressed: e-mail mwinnik@alchemy.chem.utoronto.ca.

[⊗] Abstract published in *Advance ACS Abstracts,* September 15, 1996.

S0024-9297(96)00138-6 CCC: $12.00

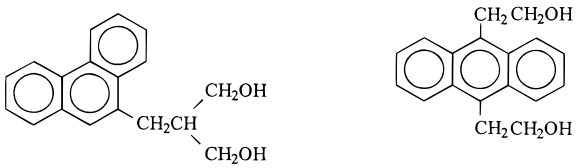

Phe-diol **An-diol**

Figure 1. Structures of Phe-diol and An-diol.

attempt to rationalize these changes in terms of the morphology of the IPN. The diol derivatives used to introduce the Phe and An groups into the PU component, Phe-diol and An-diol, are shown in Figure 1.

Experimental Section

1. Preparation of $PU^{75\%}_{g15[An/Phe0]}PA(EHA)^{100\%}PU^{100\%}$, $PU^{75\%}_{g15[An/Phe3]}PA(EHA)^{100\%}PU^{100\%}$, $PU^{75\%}_{g15[An/Phe6]}PA(EHA)^{100\%}PU^{100\%}$, $PU^{75\%}_{g15[An/Phe9]}PA(EHA)^{100\%}PU^{100\%}$, and $PU^{75\%}_{g15[An/Phe12]}PA(EHA)^{100\%}PU^{100\%}$. In making fluorescence labeled SeqIPN $PU^{75\%}_{g15}PA(EHA)^{100\%}PU^{100\%}$ samples, fluorescent compounds Phe-diol and An-diol (Figure 1 and Table 1) were added to the monomer mixture used for preparing $PU^{75\%}_{g15}PA(EHA)^{100\%}PU^{100\%}$. Five samples, $PU^{75\%}_{g15[An/Phe0]}PA(EHA)^{100\%}PU^{100\%}$, $PU^{75\%}_{g15[An/Phe3]}PA(EHA)^{100\%}PU^{100\%}$, $PU^{75\%}_{g15[An/Phe6]}PA(EHA)^{100\%}PU^{100\%}$, $PU^{75\%}_{g15[An/Phe9]}PA(EHA)^{100\%}PU^{100\%}$, and $PU^{75\%}_{g15[An/Phe12]}PA(EHA)^{100\%}PU^{100\%}$, were prepared by varying the An/Phe ratios (Table 1). These samples were made by following the same processing conditions described for $PU^{75\%}_{g15}PA(EHA)^{100\%}PU^{100\%}$ in the preceding paper,[1] except that in this case, thinner films (50−150 μm thick) were prepared on surfaces of quartz plates (1 mm × 10 mm × 25 mm) for fluorescence decay measurements, in order to avoid self-absorption of fluorescence emissions.

2. Preparation of SeqIPN $PU^{100\%}_{g180[An/Phe0]}PA(IBA)^{100\%}$, $PU^{100\%}_{g180[An/Phe3]}PA(IBA)^{100\%}$, $PU^{100\%}_{g180[An/Phe6]}PA(IBA)^{100\%}$, $PU^{100\%}_{g180[An/Phe9]}PA(IBA)^{100\%}$, and $PU^{100\%}_{g180[An/Phe12]}PA(IBA)^{100\%}$. These samples were prepared on quartz substrates as described above, by following the same processing conditions described for $PU^{100\%}_{g180}PA(IBA)^{100\%}$ in the preceding paper[1]. Monomer mixture compositions for each sample are given in Table 2.

3. Fluorescence Decay Measurements. Fluorescence decay profiles were measured by the time-correlated single-photon-counting technique and analyzed by employing the iterative reconvolution method.[3] Samples were excited at 300 nm with a pulsed D_2 lamp as the excitation source, fluorescence was detected at 366 nm, and 20000 counts were collected in the maximum channel. The instrumentation and data analysis have been described previously.[4,5]

Results and Discussion

The most common tools for investigating IPN morphology are thermal methods such as differential scanning calorimetry (DSC) and dynamic mechanical analysis (DMA), and electron microscopy, both SEM and TEM. In this way, one attempts to determine factors such as domain size and shape, phase continuity, and the T_g of each component. These global features are important determinants of IPN properties and performance.[6,7] Two other factors of great importance are the extent of phase mixing in IPN's and the sharpness or diffuseness of the interfaces between the components. Because the extent of phase separation is restricted due to the nature of the sample preparation, phase mixing should be a common property of IPN's. A common signature of phase mixing is an inward shift in the apparent T_g's of the components of an IPN.[6,7] On occasion, one observes a single T_g in IPN's formed from polymers with well-separated individual T_g's.[8,9] In systems where a single T_g is observed, one commonly interprets this result to indicate extensive mixing of the components or, in the extreme, formation of a single phase.[9]

We know relatively little about interfaces and interphases in IPN's. One might imagine that the properties of the interface are determined by thermodynamic factors, such as the Flory−Huggins χ-parameter between the two components, and by kinetic factors related to the relative kinetics of cross-linking and phase separation. To obtain this kind of information, one needs experimental techniques capable of investigating interfaces at the molecular level.

Various approaches have been taken to study the extent of phase mixing and the nature of the interfaces in IPN's. Among the most powerful are NMR methods, particularly those involving spin diffusion,[10] and X-ray and neutron scattering.[11−13] Although there have been various reports in the literature describing these measurements, the picture they provide is still far from complete.

Fluorescence techniques are often a useful alternative or a powerful complement to NMR and scattering methods. These techniques, particularly direct nonradiative energy transfer (DET) methods, are being used increasingly in polymer science to study polymer prop-

Table 1. SeqIPN $PU^{75\%}_{g15}PA(EHA)^{100\%}PU^{100\%}$ and PU Sample Compositions[1,2]

sample	urethane monomers (g)	EHA + cross-linker (g)	Phe-diol (mg)	An-diol (mg)	An/Phe ratio
$PU^{75\%}_{g15[An/Phe0]}PA(EHA)^{100\%}PU^{100\%}$	12.5	6.0	4.8	0	0
$PU^{75\%}_{g15[An/Phe3]}PA(EHA)^{100\%}PU^{100\%}$	12.5	6.0	4.8	14.4	3
$PU^{75\%}_{g15[An/Phe6]}PA(EHA)^{100\%}PU^{100\%}$	12.5	6.0	4.8	28.8	6
$PU^{75\%}_{g15[An/Phe9]}PA(EHA)^{100\%}PU^{100\%}$	12.5	6.0	4.8	43.2	9
$PU^{75\%}_{g15[An/Phe12]}PA(EHA)^{100\%}PU^{100\%}$	12.5	6.0	4.8	57.6	12
PU0	12.5	0	4.8	0	0
PU3	12.5	0	4.8	14.4	3
PU6	12.5	0	4.8	28.8	6
PU9	12.5	0	4.8	43.2	9
PU12	12.5	0	4.8	57.6	12

Table 2. SeqIPN $PU^{100\%}_{g180}PA(EHA)^{100\%}$ Compositions[1,2]

sample	urethane monomers (g)	IBA + cross-linker (g)	Phe-diol (mg)	An-diol (mg)	An/Phe ratio
$PU^{100\%}_{g180[An/Phe0]}PA(IBA)^{100\%}$	12.5	6.0	4.8	0	0
$PU^{100\%}_{g180[An/Phe3]}PA(IBA)^{100\%}$	12.5	6.0	4.8	14.4	3
$PU^{100\%}_{g180[An/Phe6]}PA(IBA)^{100\%}$	12.5	6.0	4.8	28.8	6
$PU^{100\%}_{g180[An/Phe9]}PA(IBA)^{100\%}$	12.5	6.0	4.8	43.2	9
$PU^{100\%}_{g180[An/Phe12]}PA(IBA)^{100\%}$	12.5	6.0	4.8	57.6	12

erties[14] such as conformation,[15] diffusion,[16] and morphology.[17] They have not yet been applied to the study of traditional IPN's. We have, however, used these techniques with good success to establish that a set of polymeric microspheres which we prepared by dispersion polymerization in hydrocarbon media had an IPN-like structure. In one of the most interesting of these experiments,[4] we could demonstrate phase continuity by showing that a fluorescence quencher introduced outside the particles could permeate through the minor component to reach fluorescent groups in the interior of the particles.

Here we look at structure rather than transport, using phenanthrene as the energy donor and anthracene as the energy acceptor. This pair, which has a characteristic Förster distance R_0 of 25.5 Å,[18] has been used in a number of studies of polymer systems.[15c,16,19] The attractiveness of Phe as a donor chromophore is that it is relatively insensitive to the chemical details of its surroundings and, following pulsed excitation, commonly decays to the ground state via a simple exponential decay law.

Energy Transfer in the Polyurethane Matrix. As a baseline for these experiments, we prepared a series of polyurethane samples with the same composition as the PU component of the IPN's reported here. The PU samples were labeled with the donor and acceptor diols shown in Figure 1. The sample containing only Phe exhibited an exponential decay profile. As increasing amounts of An were introduced into the sample, the profiles decayed more rapidly at early times, in a manner entirely consistent with Förster decay kinetics.[2] In such a system, with a random three-dimensional distribution of donors and acceptors, the donor fluorescence decay $I_D(t)$ is described by the Förster equation:[20]

$$I_D(t) = A \exp\left[-\frac{t}{\tau_0} - P\left(\frac{t}{\tau_0}\right)^{0.5}\right] \quad (1)$$

Here τ_0 is the donor fluorescence lifetime in the absence of acceptors, and P is proportional to the acceptor (quencher) concentration [Q]:[20,21]

$$P = \gamma \times \frac{4\pi^{3/2} N R_0^{\,3}[\mathrm{Q}]}{3000} \quad (2)$$

In eq 2, γ is an orientation factor, and N is Avogadro's number.

Systems that follow Förster kinetics involve static quenching. In such systems, one often finds that the decrease in donor fluorescence intensity caused by nonradiative energy transfer to the acceptor follows the behavior of the Perrin static quenching model.[22] This model was developed to describe static quenching between randomly distributed, immobile fluorophores and quenchers which are accidentally in proximity. Although the assumptions of the model as they were originally developed (instantaneous quenching of the donor D if the quencher is anywhere inside a quenching sphere of radius R_s centered on D*, and no quenching if Q is outside of this volume) are more restrictive than would seem necessary, Inokuti and Hirayama have shown that this type of quenching behavior is obtained for static pairs when there is a distance-dependent rate of interaction between them.[23] When Perrin kinetics are followed, one can obtain the radius of the quenching sphere R_s from data plotted according to the expression

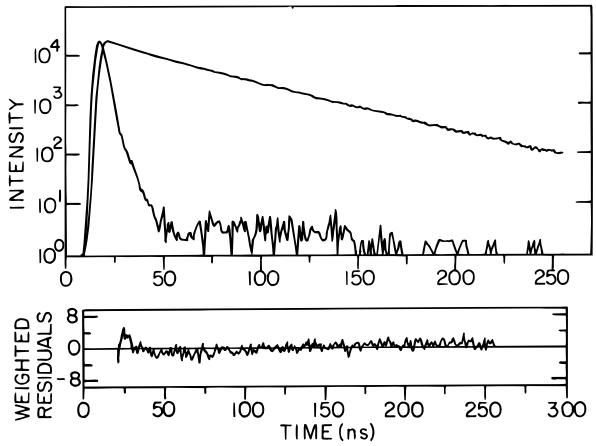

Figure 2. Fluorescence decay profile for sample $PU^{75\%}_{g15[An/Phe0]}PA(EHA)^{100\%}PU^{100\%}$ and the weighted residuals from single-exponential fit to the decay ($\tau_0 = 48.7$ ns, $\chi^2 = 1.86$).

$$\ln \frac{F_0}{F} = \frac{4}{3}\pi R_s^{\,3}[\mathrm{Q}] \quad (3)$$

where F and F_0 are defined below. In the PU samples described above, fluorescence intensities calculated by integrating the normalized fluorescence decay profiles gave an excellent fit when plotted according to eq 3, yielding a value of R_s very close to that of R_0.[2]

Part 1. Degree of Phase Mixing in SeqIPN $PU^{75\%}_{g15}PA(EHA)^{100\%}PU^{100\%}$

Fluorescence Decay Profiles for Labeled SeqIPN $PU^{75\%}_{g15}PA(EHA)^{100\%}PU^{100\%}$. The fluorescence decay profile for sample $PU^{75\%}_{g15[An/PheO]}PA(EHA)^{100\%}PU^{100\%}$, labeled only with Phe, is shown in Figure 2. The profile can be fitted to a single-exponential function to yield $\tau_0 = 48.7$ ns and $\chi^2 = 1.86$. By comparison, the Phe-labeled PU matrix exhibits an exponential decay with $\tau_0 = 49.7$ ns and $\chi^2 = 1.04$. While the overall lifetime is not very different, small deviations from exponentiallity are apparent. These deviations can be seen in the weighted residuals in Figure 2. The most serious deviations occur at early times and may be due to some scattered excitation light reaching the detector, but there is a further indication of small deviations at long times in the decay. These deviations are sufficiently small that they are difficult to interpret unambiguously. We do know that the photoinitiator introduces a low concentration of aromatic ketone groups into the acrylate phase, and these are effective (static) quenchers of phenanthrene fluorescence.[24] It may be that a very small fraction of the Phe groups are influenced by these ketone substituents on the ends of the acrylate chains. To proceed, however, it is necessary to treat the value of $\tau_0 = 48.7$ ns obtained in this experiment as the unquenched donor fluorescence lifetime.

Introduction of acceptors (An) into samples $PU^{75\%}_{g15[An/Phe3]}PA(EHA)^{100\%}PU^{100\%}$ to $PU^{75\%}_{g15[An/Phe12]}PA(EHA)^{100\%}PU^{100\%}$ enhances the phenanthrene decay rate. With increasing concentrations of An in the samples, one observes more pronounced curvature in the decay profiles and a decrease in the area under each decay curve. Similar behavior was observed in the PU samples.[2] We proceed with our analysis by comparing

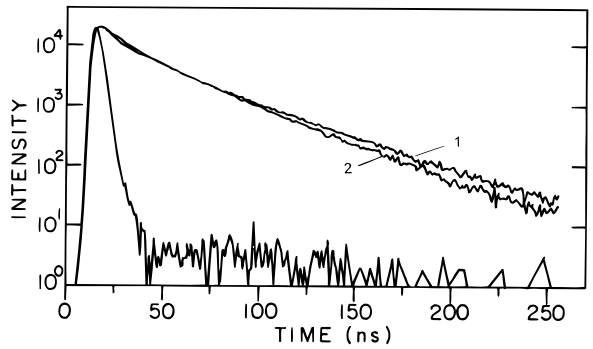

Figure 3. Fluorescence decay curves for SeqIPN $PU^{75\%}_{g15[An/Phe12]}PA(EHA)^{100\%}PU^{100\%}$ (1) and PU12 (2).

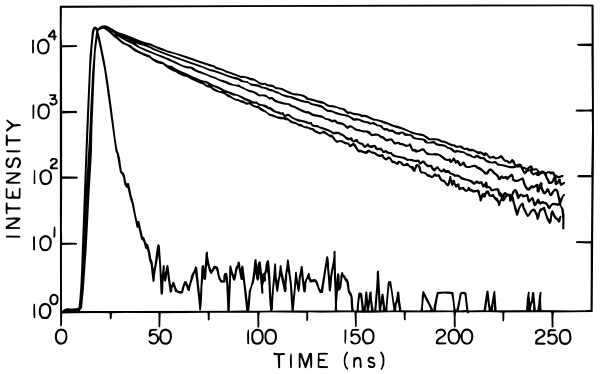

Figure 4. Fluorescence decay profiles for SeqIPN samples (from top to bottom: $PU^{75\%}_{g15[An/Phe0]}PA(EHA)^{100\%}PU^{100\%}$, $PU^{75\%}_{g15[An/Phe3]}PA(EHA)^{100\%}PU^{100\%}$, $PU^{75\%}_{g15[An/Phe6]}PA(EHA)^{100\%}PU^{100\%}$, $PU^{75\%}_{g15[An/Phe9]}PA(EHA)^{100\%}PU^{100\%}$, and $PU^{75\%}_{g15[An/Phe12]}PA(EHA)^{100\%}PU^{100\%}$).

$PU^{75\%}_{g15}PA(EHA)^{100\%}PU^{100\%}$ samples with PU samples containing similar amounts of acceptor. For example, in Figure 3, we compare fluorescence decay curves of sample $PU^{75\%}_{g15[An/Phe12]}PA(EHA)^{100\%}PU^{100\%}$ with that of PU12. Both contain the same extent of Phe and An labeling, with the labels confined to the urethane polymer. One sees that $PU^{75\%}_{g15[An/Phe12]}PA(EHA)^{100\%}PU^{100\%}$ exhibits faster decay at early times and a slower decay at later times (75−250 ns) than the PU12 sample. When the decay profiles are normalized and then integrated, one finds that the area under the $PU^{75\%}_{g15[An/Phe12]}PA(EHA)^{100\%}PU^{100\%}$ sample is significantly larger than that of the PU12 sample. This behavior is seen in all four pairs of samples with different levels of labeling by acceptor. From this qualitative examination of the decay curves, we can draw the major conclusions of this paper: in the IPN sample, there is a broader distribution of Phe/An separation distances and significantly less energy transfer. For the extent of energy transfer to *decrease* in the IPN, the urethane component must be *diluted* with acrylate polymer. This points to significant mixing of the two polymers in the system.

Fluorescence decay curves for all of the $PU^{75\%}_{g15}PA(EHA)^{100\%}PU^{100\%}$ samples are shown in Figure 4. The remainder of Part 1 in this paper is devoted to an attempt to quantify the extent of intermixing in these samples by fitting the decay curves to various models.

Data Analysis in Terms of the Perrin Model. According to eq 3, the Perrin model considers the influence of quencher concentration on the relative fluorescence intensity F_0/F of the fluorophore. In thin-film samples, the most reliable way to obtain these intensities is to integrate the normalized fluorescence decay curve.[22,25] Here we fit the decay curves to a sum of two exponential terms (Table 3), and the fluorescence intensity is given by the expression $F = A_1\tau_1 + A_2\tau_2$ (Table 4). Perrin plots of the data for the SeqIPN $PU^{75\%}_{g15}PA(EHA)^{100\%}PU^{100\%}$ samples and for the PU samples are presented in Figure 5. Note that the *x*-axis ($[An]_{PU}$) in this plot is the concentration of quencher calculated from the number of moles of An and the amount of polyurethane precursor in the system; cf. Table 1. For the isotropic PU sample, this represents the true concentration of quencher in the sample. From the smaller slope found for the SeqIPN $PU^{75\%}_{g15}PA(EHA)^{100\%}PU^{100\%}$ samples, we infer that the quencher concentration is diluted with respect to the PU sample.

To proceed with the analysis, we assume that the radius of the active quenching sphere (R_s) for the Phe/An interaction in both systems is the same and that all fluorophores are confined to, and randomly distributed within, some subset $V_{D/A}$ of the total IPN volume (V_{total}). If the volumes of the polyacrylate V_{PA} and the polyurethane V_{PU} components are additive ($V_{PA} + V_{PU} = V_{total}$), this analysis indicates that $V_{D/A} > V_{PU}$, and the following relationship is always valid (cf. Appendix II):

$$\text{An (mol) added} = [An]_{D/A} \times V_{D/A} = [An]_{PU} \times V_{PU} \quad (4)$$

$$\frac{V_{D/A}}{V_{PU}} = \frac{\text{slope(PU)}}{\text{slope(IPN)}} \quad (5)$$

From the slopes of the two Perrin plots in Figure 5, $V_{D/A}/V_{PU} = 1.34$ was obtained. This suggests that all fluorophores are distributed in a volume ($V_{D/A}$) which is larger than the volume of the original polyurethane component (V_{PU}) in the IPN. Since all fluorophores are covalently bonded only to the polyurethane network, this increase in volume of this phase must be related to polyacrylate chain interpenetration into the polyurethane-rich continuous phase.

Data Analysis in Terms of the Förster Model. In previous experiments,[2] we examined the donor fluorescence decay profiles in samples of polyurethane having the same composition as the PU component of the IPN's studied here. In those experiments, each individual Phe fluorescence decay curve gave a good fit to eq 1, and the values of *P* obtained were proportional to the global concentration of acceptor $[An]_{PU}$ in the system. These

Table 3. Parameters from Double-Exponential Fit to SeqIPN $PU^{75\%}_{g15}PA(EHA)^{100\%}PU^{100\%}$ Decay Profiles

sample	10^3[An]PU	A_1[a]	τ_1	A_2[a]	τ_2	χ^2
$PU^{75\%}_{g15[An/Phe0]}PA(EHA)^{100\%}PU^{100\%}$	0	0.874	49.5	0.126	10.6	0.97
$PU^{75\%}_{g15[An/Phe3]}PA(EHA)^{100\%}PU^{100\%}$	4.51	0.729	47.3	0.271	15.9	1.56
$PU^{75\%}_{g15[An/Phe6]}PA(EHA)^{100\%}PU^{100\%}$	9.02	0.617	44.2	0.383	14.8	1.85
$PU^{75\%}_{g15[An/Phe9]}PA(EHA)^{100\%}PU^{100\%}$	13.5	0.512	42.2	0.488	15.1	1.92
$PU^{75\%}_{g15[An/Phe12]}PA(EHA)^{100\%}PU^{100\%}$	18.0	0.443	40.7	0.557	13.9	1.86

[a] Normalized.

Table 4. Fluorescence Intensity Calculation for SeqIPN $PU^{75\%}_{g15}PA(EHA)^{100\%}PU^{100\%}$ Samples

sample	$10^3[An]_{PU}$	F	F_0	ln (F_0/F)
$PU^{75\%}_{g15[An/Phe0]}PA(EHA)^{100\%}PU^{100\%}$	0	44.6 (F_0)	44.6	0
$PU^{75\%}_{g15[An/Phe3]}PA(EHA)^{100\%}PU^{100\%}$	4.51	38.8	44.6	0.139
$PU^{75\%}_{g15[An/Phe6]}PA(EHA)^{100\%}PU^{100\%}$	9.02	32.9	44.6	0.303
$PU^{75\%}_{g15[An/Phe9]}PA(EHA)^{100\%}PU^{100\%}$	13.5	29.0	44.6	0.431
$PU^{75\%}_{g15[An/Phe12]}PA(EHA)^{100\%}PU^{100\%}$	18.0	25.7	44.6	0.549

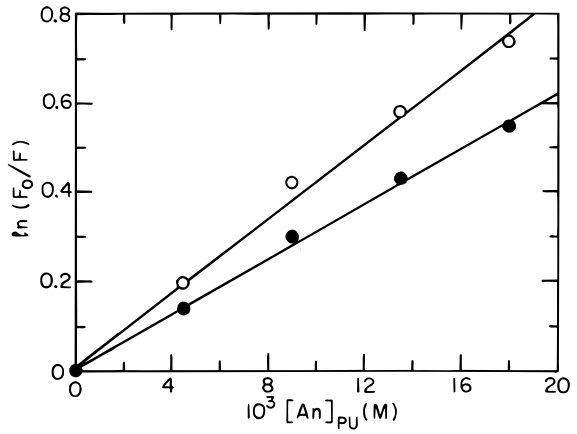

Figure 5. Perrin plots for SeqIPN $PU^{75\%}_{g15}PA(EHA)^{100\%}PU^{100\%}$ (filled symbol) and PU samples (open symbol).

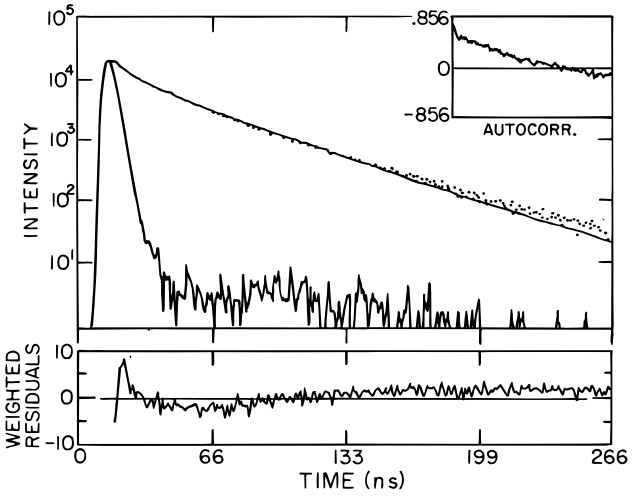

Figure 6. Förster equation fit to SeqIPN $PU^{75\%}_{g15[An/Phe12]}PA(EHA)^{100\%}PU^{100\%}$ decay.

results serve as the basis of comparison for the data obtained here.

The IPN fluorescence decay profiles (Figure 4) were fitted to the Förster expression, eq 1. The fit of the data for sample $PU^{75\%}_{g15[An/Phe12]}PA(EHA)^{100\%}PU^{100\%}$ is shown in Figure 6, and the corresponding weighted residuals are plotted in Figure 7. Relatively high χ^2 values (3−4) and relatively large weighted residuals were observed, particularly in the early channels (Figure 7).

To further analyze the data-fitting process, we examine more closely the Förster expression fit to the $PU^{75\%}_{g15[An/Phe12]}PA(EHA)^{100\%}PU^{100\%}$ decay shown in Figure 6. Deviations from the fit occur both in the tail of the decay curve and at very early times. Deviations from Förster model fitting, in terms of χ^2 and the magnitude of weighted residuals, increase with the increase of quencher concentration. In Figure 3, we compare the shape of the decay profile for this sample

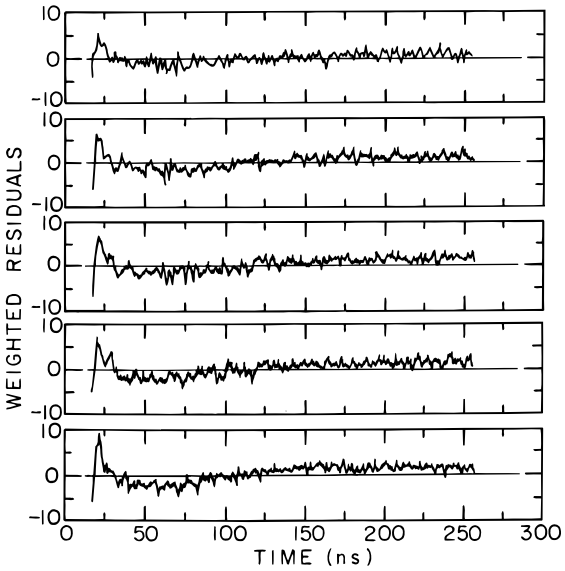

Figure 7. Weighted residuals from Förster eq 1 fit to SeqIPN decays (from top to bottom: $PU^{75\%}_{g15[An/Phe0]}PA(EHA)^{100\%}PU^{100\%}$, $PU^{75\%}_{g15[An/Phe3]}PA(EHA)^{100\%}PU^{100\%}$, $PU^{75\%}_{g15[An/Phe6]}PA(EHA)^{100\%}PU^{100\%}$, $PU^{75\%}_{g15[An/Phe9]}PA(EHA)^{100\%}PU^{100\%}$, $PU^{75\%}_{g15[An/Phe12]}PA(EHA)^{100\%}PU^{100\%}$).

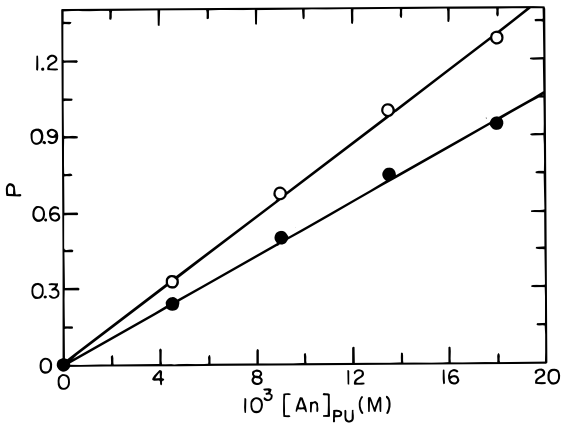

Figure 8. *P* vs $[An]_{PU}$ plots for SeqIPN $PU^{75\%}_{g15}PA(EHA)^{100\%}PU^{100\%}$ (filled symbol) and PU samples (open symbol).

with that of PU12, containing the same amount of An per volume of PU. A faster decay of the $PU^{75\%}_{g15[An/Phe12]}PA(EHA)^{100\%}PU^{100\%}$ fluorescence intensity occurs in the early (first 20) channels, compared with the decay of the PU12 sample. More rapid decay points to the contribution of donors surrounded by a higher local concentration of acceptors than in the PU sample. One also observes a longer tail in the decay of the $PU^{75\%}_{g15[An/Phe12]}PA(EHA)^{100\%}PU^{100\%}$ sample. This observation suggests that some donors in the IPN sample are surrounded by a lower local concentration of acceptor than in the PU12 sample. Taken together, we infer from these differences that the distribution of donors and acceptors is broader in the IPN sample than in the PU sample. A better fit to the decay curves should be obtained if one could derive an energy transfer kinetic expression with an appropriate distribution function for the Phe/An groups across the PU/PA interface.

P values were obtained from the fits, and it is interesting to note that the *P* vs [An] plot is still linear with good precision (Figure 8), despite the deviations in the individual fits. The *P* values are listed in Table 5. In plotting the data in Figure 8, to facilitate

Table 5. Parameters from Förster Eq 1 Fitting to IPN $PU^{75\%}_{g15}PA(EHA)^{100\%}PU^{100\%}$ Decay Profiles

sample	$10^3[An]_{PU}$	P	τ_0 (fixed)	χ^2
$PU^{75\%}_{g15[An/Phe0]}PA(EHA)^{100\%}PU^{100\%}$	0	0.00917	48.7	1.75
$PU^{75\%}_{g15[An/Phe3]}PA(EHA)^{100\%}PU^{100\%}$	4.51	0.238	48.7	3.11
$PU^{75\%}_{g15[An/Phe6]}PA(EHA)^{100\%}PU^{100\%}$	9.02	0.503	48.7	3.31
$PU^{75\%}_{g15[An/Phe9]}PA(EHA)^{100\%}PU^{100\%}$	13.5	0.752	48.7	3.54
$PU^{75\%}_{g15[An/Phe12]}PA(EHA)^{100\%}PU^{100\%}$	18.0	0.947	48.7	4.24

comparison with the previous experiments on the pure PU component, we choose $[An]_{PU}$ as the *x*-axis and calculate $[An]_{PU}$ by dividing the number of moles of An in the system by the predicted volume of the PU component in the IPN. We conclude from this Förster model analysis that the fluorophores are not randomly distributed in the IPN samples; therefore the *P* parameter represents an averaged acceptor concentration in the portion of the sample in which the chromophores are located.

To proceed with our analysis, we compare the values of the *P* parameter obtained from the IPN samples to those obtained from the PU samples. Here we assume that the Förster energy transfer critical radius R_0 is the same in both the IPN and the polyurethane network. Once again, the slope for the data from the PU samples is greater than that for the IPN samples (Figure 8). Smaller values of *P* indicate less fluorescence quenching in the IPN samples, consistent with dilution of the chromophores in the IPN relative to the PU matrix. By applying the same analysis method used in the Perrin plot section above, we calculate from the slope ratios that $V_{D/A}/V_{PU} = 1.36$.

IPN Morphology Analysis. In SeqIPN $PU^{75\%}_{g15}PA(EHA)^{100\%}PU^{100\%}$ samples, both the Perrin model and the Förster model reveal that the acceptor concentration $[An]_{D/A}$ inferred from the experimental data is more dilute than that one would obtain if the chromophores remained confined to the PU phase. This 34−36% dilution factor strongly suggests some miscibility of the polyacrylate with the polyurethane, increasing the volume of this phase and thereby increasing as well the mean separation of the chromophores. A simple analysis of the dilution effect can be developed as follows: Assuming additive volumes, the total volume of the sample $V_{total} = V_{PU} + V_{PA}$, where V_{PU} and V_{PA} refer to the volumes anticipated from polymerization of the individual components. Similarly, $V_{total} = V_{D/A} + V'_{PA}$, where V'_{PA} now refers to the discrete unmixed PA phase in the final IPN. By definition, based upon the fluorescence results, this is the domain which excludes the fluorescent labels. From this analysis, we calculate that about 70% of the polyacrylate interpenetrates into polyurethane-rich continuous phase, and the remaining 30% of the polyacrylate (PA′) forms the dispersed phase. In the preceding paper,[1] good phase mixing (single T_g) and very small phase domains (<20 nm) were observed for this SeqIPN system. We now suggest that the small discrete phases observed in the TEM images for this IPN $PU^{75\%}_{g15}PA(EHA)^{100\%}PU^{100\%}$ correspond to the dispersed PA′ phase.

This type of IPN morphology resembles that of a poly(ethyl acrylate)−PMMA IPN reported by Sperling and co-workers more than 20 years ago.[26] Sperling and coworkers proposed a *wall and cell* model to describe polymer chain interpenetration on the molecular or segmental level.[26] This wall and cell model predicts that the dispersed phases are virtually interconnected by their own polymer chains, which interpenetrate through the continuous phase (Figure 9).[6,26] Note that these interpenetrated polymer chains will increase the volume of the continuous phase. This wall and cell model facilitates our data interpretation. In terms of this model, in SeqIPN $PU^{75\%}_{g15}PA(EHA)^{100\%}PU^{100\%}$, about 70% of the polyacrylate serve as connecting chains, interpenetrated into the polyurethane-rich continuous phase, and 30% of the polyacrylate form the nodules of the dispersed phase.

Figure 9. IPN wall and cell model.

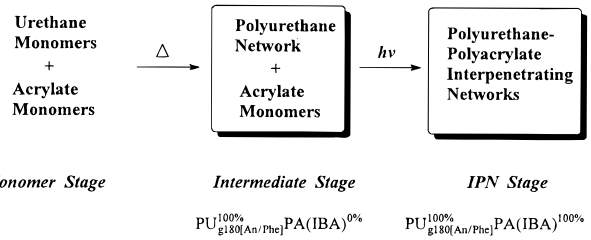

Figure 10. Preparation of SeqIPN $PU^{100\%}_{g180[An/Phe]}PA(IBA)^{100\%}$.

It would be useful to compare the extent of mixing calculated from energy transfer experiments with that estimated in the previous paper from shifts in tan δ in DMA measurements. In the specific case described above, this comparison is not possible. The T_g values of the PU and PEHA components are too similar for meaningful information to be obtained by DMA. This type of analysis is possible only for the PU−PIBA system, where the individual T_g's are well separated.

Part 2. Energy Transfer Studies in SeqIPN $PU^{100\%}_{g180}PA(IBA)^{100\%}$

In the preceding paper,[1] we described a series of PIBA IPN samples, of which SeqIPN $PU^{100\%}_{g180}PA(IBA)^{100\%}$ exhibited the greatest the degree of phase mixing. The extent of phase mixing in this sample could be estimated from DMA experiments. Here we compare the results of DET experiments with the DMA results. In fact a more thorough analysis of mixing can be carried out, made possible by the insensitivity of phenanthrene fluorescence to quenching by acrylate esters. We can label the PU phase with both phenanthrene and anthracene and study the energy transfer in the *intermediate stage* [$PU^{100\%}_{g180[An/Phe]}PA(IBA)^{0\%}$] (cf. Figure 10) where the PU phase is swollen by acrylate monomer. This can be compared to the fully cured IPN to assess the timing and extent of demixing in the system.

Energy Transfer in the Intermediate Stage. At the intermediate stage of IPN formation, the polyurethane network has been formed but remains swollen by

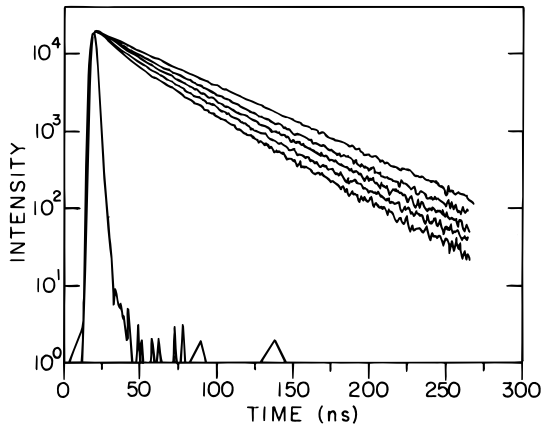

Figure 11. Fluorescence decay profiles from the intermediate stage (from top to bottom: $PU^{100\%}_{g180[An/Phe0]}PA(IBA)^{0\%}$, $PU^{100\%}_{g180[An/Phe3]}PA(IBA)^{0\%}$, $PU^{100\%}_{g180[An/Phe6]}PA(IBA)^{0\%}$, $PU^{100\%}_{g180[An/Phe9]}PA(IBA)^{0\%}$, and $PU^{100\%}_{g180[An/Phe12]}PA(IBA)^{0\%}$).

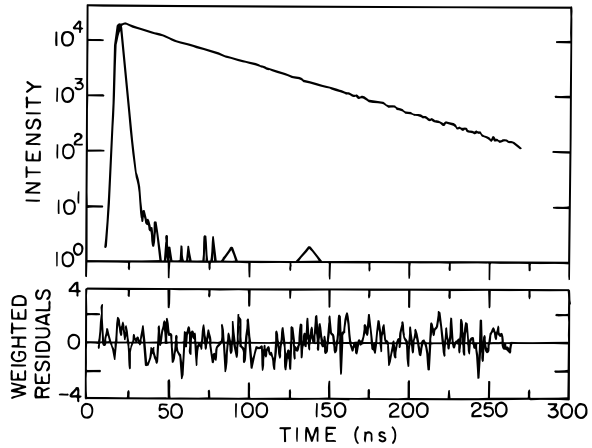

Figure 12. Fluorescence decay profile for sample $PU^{100\%}_{g180[An/Phe0]}PA(IBA)^{0\%}$ and the weighted residuals from single-exponential fit to the decay ($\tau_0 = 48.7$ ns, $\chi^2 = 0.98$).

the acrylate monomers. One anticipates that this swelling will increase the distance between donors and acceptors, leading to a decrease in the efficiency of energy transfer relative to that of the pure PU component. Fluorescence decays at this intermediate stage are presented in Figure 11. These decays are analyzed as described above in terms of both the Förster equation and the Perrin model of static quenching.

The fluorescence decay profile for sample $PU^{100\%}_{g180[An/Phe0]}PA(IBA)^{0\%}$, labeled with only Phe, is shown in Figure 12. This profile fits well to a single-exponential decay function to yield $\tau_0 = 48.7$ ns and $\chi^2 = 0.98$. The introduction of acceptors (An) enhances the phenanthrene decay rate (Figure 11). Similar behavior is also observed in the corresponding unswollen PU samples. For comparable levels of acceptor labeling, however, the fluorescence of the PU samples decays faster than that of the corresponding $PU^{100\%}_{g180[An/Phe]}PA(IBA)^{0\%}$ samples.

Data Analysis in Terms of the Förster Model. The fluorescence decay profiles in Figure 11 were fitted to the Förster equation, eq 1, with $\chi^2 < 1.3$ for all samples (Table 6). The P parameters are plotted against $[An]_{PU}$ in Figure 13. From eq 5, we obtain $V_{D/A}/V_{PU} = 1.53$, which implies that all acrylate monomers are intimately mixed with the PU network.

Data Analysis in Terms of the Perrin Model. In order to use the Perrin model (eq 3), we need to know

Table 6. Parameters from Förster Eq 1 Fitting to $PU^{100\%}_{g180[An/Phe]}PA(IBA)^{0\%}$ Decay Profiles

sample	$10^3[An]_{PU}$	P	τ_0(fixed)	χ^2
$PU^{100\%}_{g180[An/Phe0]}PA(IBA)^{0\%}$	0	3.6×10^{-4}	48.7	0.93
$PU^{100\%}_{g180[An/Phe3]}PA(IBA)^{0\%}$	4.51	0.250	48.7	1.12
$PU^{100\%}_{g180[An/Phe6]}PA(IBA)^{0\%}$	9.02	0.448	48.7	1.21
$PU^{100\%}_{g180[An/Phe9]}PA(IBA)^{0\%}$	13.5	0.640	48.7	1.21
$PU^{100\%}_{g180[An/Phe12]}PA(IBA)^{0\%}$	18.0	0.865	48.7	1.26

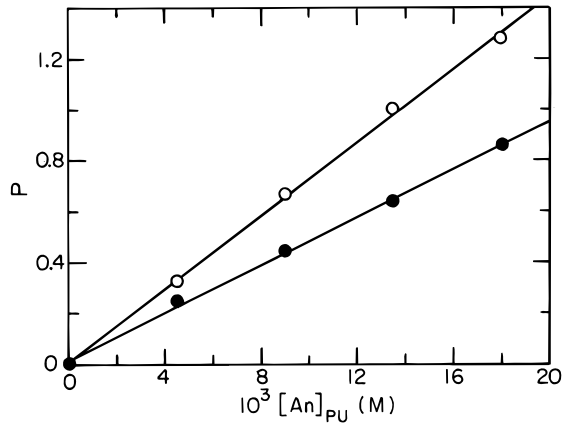

Figure 13. P vs $[An]_{PU}$ plots for $PU^{100\%}_{g180[An/Phe]}PA(IBA)^{0\%}$ (filled symbol) and PU samples (open symbol).

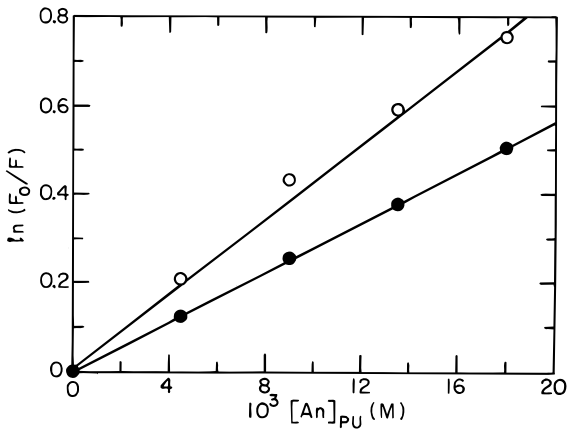

Figure 14. Perrin plots for $PU^{100\%}_{g180[An/Phe]}PA(IBA)^{0\%}$ (filled symbol) and PU samples (open symbol).

the F_0/F values at each [An] concentration. We obtain the F_0/F values by integrating the areas under the normalized fluorescence decay curves. The Perrin plot for $PU^{100\%}_{g180[An/Phe]}PA(IBA)^{0\%}$ samples are presented in Figure 14. From the slope ratios, we obtain $V_{D/A}/V_{PU} = 1.51$, which is very close to the value obtained from fitting the decay curves to the Förster model ($V_{D/A}/V_{PU} = 1.53$). From these experiments, we conclude that at this stage of the reaction, the PU phase is homogeneously swollen with acrylate monomer.

Energy Transfer in the IPN. The samples described above were exposed to UV irradiation to polymerize the PA component. Fluorescence decay profiles for SeqIPN $PU^{100\%}_{g180[An/Phe]}PA(IBA)^{100\%}$ samples are given in Figure 15. The fluorescence decay profile for $PU^{100\%}_{g180[An/Phe0]}PA(IBA)^{100\%}$, labeled with only Phe, can be fitted to an exponential decay function to yield $\tau_0 = 49.0$ ns but with $\chi^2 = 1.51$. Curing the PA component, even in the case of the donor-only labeled samples, leads to a significant increase in χ^2. These decay profiles were also analyzed in terms of the Förster model and the Perrin model, and the results are summarized below.

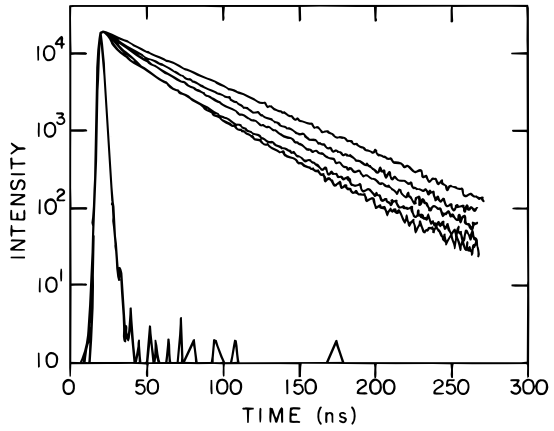

Figure 15. Fluorescence decay profiles for SeqIPN $PU^{100\%}_{g180[An/Phe]}PA(IBA)^{100\%}$ (from top to bottom: $PU^{100\%}_{g180[An/Phe0]}PA(IBA)^{100\%}$, $PU^{100\%}_{g180[An/Phe3]}PA(IBA)^{100\%}$, $PU^{100\%}_{g180[An/Phe6]}PA(IBA)^{100\%}$, $PU^{100\%}_{g180[An/Phe9]}PA(IBA)^{100\%}$, and $PU^{100\%}_{g180[An/Phe12]}PA(IBA)^{100\%}$).

Table 7. Parameters from Förster Eq 1 Fitting to SeqIPN $PU^{100\%}_{g180[An/Phe]}PA(IBA)^{100\%}$ Decay Profiles

sample	10^3[An]	P	τ_0(fixed)	χ^2
$PU^{100\%}_{g180[An/Phe0]}PA(IBA)^{100\%}$	0	$\tau_0 = 49.0$ ns		1.51
$PU^{100\%}_{g180[An/Phe3]}PA(IBA)^{100\%}$	4.51	0.246	48.7	2.08
$PU^{100\%}_{g180[An/Phe6]}PA(IBA)^{100\%}$	9.02	0.469	48.7	2.02
$PU^{100\%}_{g180[An/Phe9]}PA(IBA)^{100\%}$	13.5	0.668	48.7	4.65
$PU^{100\%}_{g180[An/Phe12]}PA(IBA)^{100\%}$	18.0	0.895	48.7	3.19

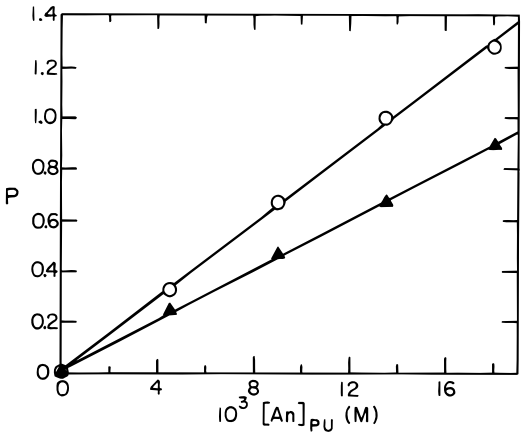

Figure 16. P vs $[An]_{PU}$ plots for $PU^{100\%}_{g180[An/Phe]}PA(IBA)^{100\%}$ (filled symbol) and PU samples (open symbol).

Fitting these decay profiles to the Förster equation led to relatively large χ^2 values (Table 7). However, the P values are still proportional to $[An]_{PU}$ (Figure 16). From eq 5 we obtain $V_{D/A}/V_{PU} = 1.47$. The Perrin plot for SeqIPN $PU^{100\%}_{g180[An/Phe]}PA(IBA)^{100\%}$ is given in Figure 17, and we obtain from the slope ratios $V_{D/A}/V_{PU} = 1.41$.

Comparison of DET and DMA Results on Phase Composition. Energy transfer studies at both the intermediate stage and the IPN stage indicate that the fluorophores covalently bound to the PU polymer are distributed in a volume ($V_{D/A}$) which is larger than the volume V_{PU} of urethane itself (cf. Table 8). Full mixing corresponds to $V_{total} = 1.5V_{PU}$: the IPN's consist of 67 wt% of PU and 33 wt % of PA (of comparable density), and we assume that $V_{total} = V_{PU} + V_{PA} = V_{PU} + 0.5V_{PU} = 1.5V_{PU}$. In the intermediate stage, we find $V_{D/A} = 1.51V_{PU}$ and $1.53V_{PU}$ respectively from the two models, and thus $V_{D/A} \approx V_{total}$. This indicates intimate and complete mixing of the acrylate monomers with the polyurethane network. At the IPN stage, $V_{D/A} < V_{total}$, which implies that some portion of the PA is not intimately mixed with the PU network. We calculate that about 80% of the PA chains are mixed with PU. The calculated extent of phase mixing for this sample is presented in Table 9 and compared with the result calculated from the DMA experiments. The results are remarkably close, although one infers a slightly smaller extent of mixing from the DMA results.

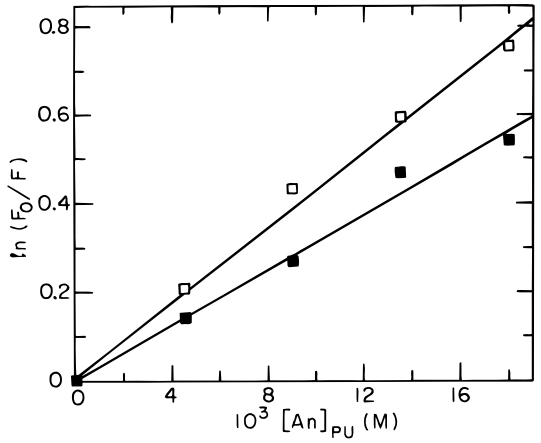

Figure 17. Perrin plots for $PU^{100\%}_{g180[An/Phe]}PA(IBA)^{100\%}$ (filled symbol) and PU samples (open symbol).

Table 8. Calculated V_{DA}/V_{PU} in Three Systems

	$V_{D/A}/V_{PU}$	
sample	Förster model	Perrin model
PU	1	1
$PU^{100\%}_{g180[An/Phe]}PA(IBA)^{0\%}$	1.53	1.51
$PU^{100\%}_{g180[An/Phe]}PA(IBA)^{100\%}$	1.47	1.41

Table 9. Degree of Phase Mixing in SeqIPN $PU^{100\%}_{g180}PA(IBA)^{100\%}$

	PU-rich phase compositions	
method	PU (wt %)	PA (wt %)
Förster model	70	30
Perrin model	72	28
DMA calculation	78	22

Summary

Fluorescence decay profiles for donor−acceptor labeled SeqIPN $PU^{75\%}_{g15}PA(EHA)^{100\%}PU^{100\%}$ samples were analyzed with the Perrin model for static quenching and the Förster model for energy transfer. By comparing the results for $PU^{75\%}_{g15}PA(EHA)^{100\%}PU^{100\%}$ with those for pure polyurethane network (PU), differences in acceptor concentration were found between these two types of samples. Partial miscibility of the PA with the PU phase serves to dilute the dyes attached to the PU component. From analysis of the fluorescence decay profiles in terms of apparent acceptor concentration in the system, it was found that 70% of the polyacrylate had interpenetrated into the polyurethane continuous phase, and the remaining 30% of the polyacrylate formed the dispersed phase. These results are consistent with the IPN wall and cell model proposed several years ago by Sperling.[26]

Such a dilution phenomenon has also been observed in another SeqIPN $PU^{100\%}_{g180}PA(IBA)^{100\%}$, and the degree of phase mixing obtained by DET experiments is supported by TEM and DMA results. In addition, DET studies at the intermediate stage $PU^{100\%}_{g180}PA(IBA)^{0\%}$

provide an insight into IPN morphology development. We document full mixing of the PU phase with acrylate monomer prior to photoinitiation of acrylate polymerization, followed by partial demixing during the second-stage polymerization.

As a final comment, we note that there is a greater degree of mixing of the PU phase with PIBA ($V_{D/A}/V_{PU})_{Perrin} = 1.41$) than with PEHMA ($(V_{D/A}/V_{PU})_{Perrin} = 1.34$). This is consistent with the greater polarity and higher solubility parameter of IBA than EHMA.

Acknowledgment. The Toronto authors thank 3M, 3M Canada Inc., and NSERC Canada for their financial support of this research.

Appendix I. IPN Notations

For general IPN notations, please see the preceding paper. Explained here are two examples of IPN with fluorescent dyes.

$PU^{75\%}_{g15[An/Phe12]}PA(EHA)^{100\%}PU^{100\%}$ stands for a SeqIPN $PU^{75\%}_{g15}PA(EHA)^{100\%}PU^{100\%}$ in which the fluorescent dyes (Phe and An) are in the PU network and the An/Phe ratio is 12.

$PU^{75\%}_{g15[An/Phe0]}PA(EHA)^{100\%}PU^{100\%}$ stands for a SeqIPN $PU^{75\%}_{g15}PA(EHA)^{100\%}PU^{100\%}$ in which the fluorescent dyes (Phe and An) are in the PU network and the An/Phe ratio is 0. This sample is labeled only with phenanthrene (Phe).

Appendix II

An example for deriving eq 5 with the Perrin equation, eq 3, is given below.

In IPN and PU samples, the Perrin plots are the following:

$$\left(\ln \frac{F_0}{F}\right)_{PU} = \frac{4}{3}\pi R_s^3[An]_{PU} = \text{slope(PU)}[An]_{PU} \quad (6)$$

$$\left(\ln \frac{F_0}{F}\right)_{IPN} = \frac{4}{3}\pi R_s^3[An]_{D/A} = \text{slope(IPN)}[An]_{PU} \quad (7)$$

By combining eqs 4, 6, and 7, eq 5 is obtained.

$$\frac{[An]_{PU}}{[An]_{D/A}} = \frac{\text{slope(PU)}}{\text{slope(IPN)}} = \frac{V_{D/A}}{V_{PU}} \quad (8)$$

References and Notes

(1) Yang, J.; Winnik, M. A.; Ylitalo, D.; DeVoe, R. J. *Macromolecules* **1996**, *29*, 7047.
(2) Yang, J.; Winnik, M. A. *Can. J. Chem.* **1995**, *73*, 1823.
(3) O'Connor, D. V.; Philips, D. *Time-Correlated Single Photon Counting*; Academic Press: London, 1984.
(4) (a) Pekcan, O.; Egan, L. S.; Winnik, M. A.; Croucher, M. D. *Macromolecules* **1990**, *23*, 2210. (b) Pekcan, O.; Winnik, M. A.; Croucher, M. D. *Macromolecules* **1990**, *23*, 2673.
(5) Wang, Y.; Zhao, C.; Winnik, M. A. *J. Chem. Phys.* **1991**, *95*, 2143.
(6) Sperling, L. H. *Interpenetrating Polymer Networks and Related Materials*; Plenum Press: New York, 1981.
(7) *Advances in Interpenetrating Polymer Networks*; Klempner, D., Frisch, K. C., Eds.; Technomic Publishing Co.: Lancaster, PA, 1989; Vol. I−III.
(8) Huelck, V.; Thomas, D. A.; Sperling, L. H. *Macromolecules* **1972**, *5*, 348.
(9) (a) Singh, S.; Frisch, H. L.; Ghiradella, H. *Macromolecules* **1990**, *23*, 375. (b) Zhou, P.; Xu, Q.; Frisch, H. L. *Macromolecules* **1994**, *27*, 938.
(10) Parizel, N.; Meyer, G.; Weill, G. *Polymer* **1995**, *36*, 2323; **1993**, *34*, 2495.
(11) Pandit, S. B.; Nadkarni, V. M. *Macromolecules* **1994**, *27*, 4583.
(12) Russell, T. P.; Lee, D. S.; Nishi, T.; Kim, S. C. *Macromolecules* **1993**, *26*, 1922.
(13) Shilov, V. V.; Lipatov, Y. S.; Karabanova, L. V.; Sergeeva, L. M. *J. Polym. Sci., Polym. Chem. Ed.* **1979**, *17*, 3083.
(14) Morawetz, H. *Science* **1988**, *240*, 172.
(15) (a) Stryer, L. *Annu. Rev. Biochem.* **1978**, *47*, 819. (b) Haas, E. In *Photophysical and Photochemical Tools in Polymer Science*; Winnik, M. A., Ed.; NATO ASI Series C182; Reidel: Dordrecht, The Netherlands, 1985; p 325. (c) Ng, D.; Guillet, J. E. *Macromolecules* **1982**, *15*, 724, 728. (d) Pispisa, B.; Venanzi, M.; Palleschi, A.; Zanotti, G. *Macromolecules* **1994**, *27*, 7800. (e) Wang, Y.; Kausch, C. M.; Chun, M.; Quirk, R. P.; Mattice, W. L. *Macromolecules* **1995**, *28*, 904.
(16) (a) Wang, Y.; Winnik, M. A. *J. Phys. Chem.* **1993**, *97*, 2507. (b) Wang, Y.; Winnik, M. A. *Macromolecules* **1993**, *26*, 3147. (c) Liu, Y. S.; Li, L.; Ni, S.; Winnik, M. A. *Chem. Phys.* **1993**, *177*, 579. (d) Dhinojwala, A.; Torkelson, J. M. *Macromolecules* **1994**, *27*, 4817.
(17) (a) Drake, J. M.; Klafter, J.; Levitz, P. *Science* **1991**, *251*, 1574. (b) Mikes, F.; Morawetz, H.; Dennis, K. S. *Macromolecules* **1984**, *17*, 60. (c) Wang, Y.; Morawetz, H. *Macromolecules* **1990**, *23*, 1753. (d) Ni, S.; Zhang, P.; Wang, Y.; Winnik, M. A. *Macromolecules* **1994**, *27*, 5742.
(18) Berlman, I. B. *Energy Transfer Parameters of Aromatic Compounds*; Academic Press: New York, 1973.
(19) Mendelsohn, A. S.; de la Cruz, M. O.; Torkelson, J. M. *Macromolecules* **1993**, *26*, 6789.
(20) (a) Förster, T. *Discuss. Faraday Soc.* **1959**, **27**, 7. (b) Birks, J. B. *Photophysics of Aromatic Molecules*; Wiley-Interscience: New York, 1970.
(21) Baumann, J.; Fayer, M. D. *J. Chem. Phys.* **1986**, *85*, 4087.
(22) Perrin, F. *Compt. Rend.* **1924**, *178*, 1978.
(23) Inokuti, M.; Hirayama, F. *J. Chem. Phys.* **1965**, *43*, 1978.
(24) Phenanthrene is particularly sensitive to quenching by ketones. We found that phenanthrene labeled in polyacrylate network was quenched by aromatic ketone groups introduced by the photoinitiator used. Cf.: Yang, J.; Winnik, M. A. *Chem. Phys. Lett.* **1995**, *238*, 25. Reference 19 also reported nonexponential decays of Phe emission in polyisoprene, which may be due to adventitious ketone groups in the polymer formed through oxidation.
(25) Eisenthal, K. B.; Siegel, S. *J. Chem. Phys.* **1964**, *41*, 652.
(26) Huelck, V.; Thomas, D. A.; Sperling, L. H. *Macromolecules* **1972**, *5*, 340.

MA960138V